



Quinoxaline Derivatives as Corrosion Inhibitors of Carbon Steel in Hydrochloridric Acid Media: Electrochemical, DFT and Monte Carlo simulations studies

Y. EL Aoufir^{1,2*}, H. Lgaz^{1,3}, H. Bourazmi², Y. Kerroum², Y. Ramli⁴, A. Guenbour², R. Salghi⁴, F. El-Hajjaji⁵, B. Hammouti⁶, H. Oudda¹

¹Laboratory of separation processes, Faculty of Science, University Ibn Tofail PO Box 242, Kenitra, Morocco

²Materials, Nanotechnology and Environment Laboratory, Faculty of Sciences, Rabat, Morocco

³Laboratory of Applied Chemistry and Environment, ENSA, Ibn Zohr University, PO Box 1136, 80000 Agadir, Morocco

⁴Medicinal Chemistry Laboratory, Faculty of Medicine and Pharmacy, Mohammed V University, 10170 Rabat, Morocco

⁵Laboratoire d'Ingénierie d'Electrochimie, Modélisation et d'Environnement (LIEME), Faculté des sciences, Université Sidi Mohammed Ben Abdellah, Fès, Maroc.

⁶Laboratoire de chimie analytique appliquée, matériaux et environnement (LC2AME), Faculté des Sciences, Université Mohammed Premier, 60000 Oujda, Morocco.

Received 28 Jun 2015, Revised 20 Sep 2016, Accepted 26 Sep 2016

*For correspondence: EL AOUFIR Yasmina: Email: eyasminal@gmail.com

Abstract

(E)-3-(4-methoxystyryl)-7-methylquinoxalin-2(1H)-one (SMQ) and 2-(4-methoxyphenyl)-7-methyl-thieno[3,2-b] quinoxaline (TMQ) are new compounds of the quinoxaline derivative family, were synthesized and tested on the corrosion of carbon steel in chlorhydric acid molar media at 303 K, using various electrochemical methods (polarization curves (PDP) and electrochemical impedance spectroscopy (EIS)). For each concentration, the protective power of both the compounds tested increase with increasing of inhibitor concentration. TMQ is more efficient than SMQ in the medium studied; these results clearly show that the TMQ is the best inhibitor. The polarization curves studies show that both compounds tested are mixed-type inhibitor in 1 M HCl media. The inhibitors react by adsorption according to Langmuir isotherm. The Nyquist curves presented a single capacitive loop, their diameter increases progressively with both inhibitors concentration. The double layer formed due to the increase in the charge transfer resistance. DFT and Monte Carlo simulation studies are in good correlation with the experimental results.

Keywords: Carbon steel; Fukui function; DFT; Corrosion inhibition; Quinoxaline; Monte Carlo simulation

1. Introduction

The steels are widely used in many industrial fields such as petroleum, chemical, and electro-chemical; but their tendency to corrosion. In industry, the acidic mediums are used to remove scale on metal surfaces [1,2]. Due to higher soluble ferrous chloride, Hydrochloridric acid is often used. Among the steel protective means against corrosion is the use of corrosion inhibitors. The organic inhibitors containing heteroatom are frequently used in order to minimize the corrosion attack on carbon steel in the acidic medium tested [3-12]. The organic inhibitors containing heteroatoms for example multiple bonds, O, N and S, are well-known inhibitors, because they allow adsorption on the steel surface [13-15]. The molecules that, together, contain sulfur and nitrogen in their structure is of particular importance, as they give a very good inhibition compared to compounds which contain sulfur or nitrogen. Recently, in addition to experimental investigations, the evaluation of inhibition performance is also conducted theoretically by DFT calculation and molecular dynamic simulation studies for the understanding of some experimentally unknown properties, exploring and establishing relationships between inhibitor molecules and the metal surface [16,17]. N.A. Al-Mobarak et al., [18] have studied the corrosion inhibition of copper in 3.5 % NaCl using new pyrimidine derivatives, namely, 2-mercapto-4-(p-methoxyphenyl)

-6-oxo-1,6-dihydropyrimidine-5-carbonitrile (MPD) by Monte Carlo simulation and theoretical calculation, and all quantum analysis correlated well with electrochemical investigation. In addition, Youguo Yan et al,[19] have applied the DFT method using the GGA/PW91 functional with the double numerical plus d-functions basis set to investigate the adsorption behavior of three purine compounds, A, B and C on the Fe (0 0 1) surface. The theoretical results, including global molecular reactivity descriptors and active sites by Fukui functions analysis well support the order of the *IE* %. They also applied molecular dynamic simulation to predict the inhibitive performance of purines studied, the tested molecules adsorbed parallel onto Fe (0 0 1) surface, and the order of interaction energy support the experimental *IE* %.

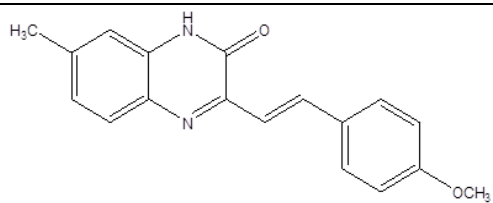
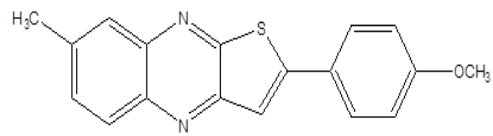
The objective of this investigation was to study the inhibitive properties of inhibition of (E)-3-(4-methoxystyryl)-7-methylquinoline-2(1H)-one (SMQ) and 2-(4-methoxy-phenyl)-7-methylthieno [3,2-b] quinoxaline (TMQ). The temperature effect on the corrosion of carbon steel in chlorhydric acid was also studied. These experiments were carried out using potentiodynamic polarization (*PDP*) curves and electrochemical impedance spectroscopy (EIS). The quantum chemical and Monte Carlo simulations studies were performed to explain the experimental results and the adsorption mechanism of tested inhibitors.

2. Experimental details

2.1. Material preparation and inhibitors

The chemical formulas of both inhibitors are grouped in the table.1. The concentration tested ranges between 10^{-3} and 10^{-6} M. Corrosive solutions were prepared by dilution of an analytical reagent grade 37% HCl with doubly distilled water.

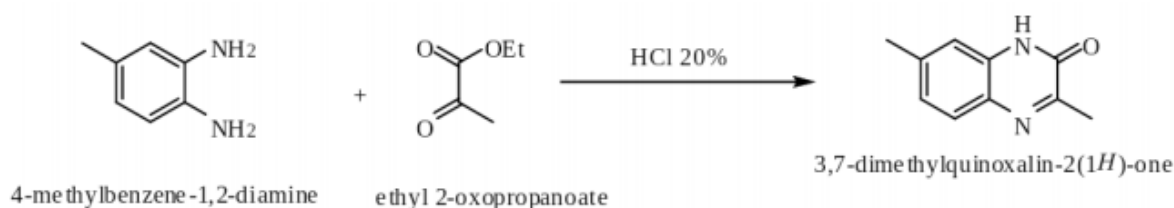
Table 1. Names and chemical structures of the organic compounds investigated

Abbreviation	Structural formula
SMQ	 (E)-3-(4-methoxystyryl)-7-methylquinoxalin-2(1H)-one
TMQ	 2-(4-methoxyphenyl)-7-methylthieno[3,2-b] quinoxaline

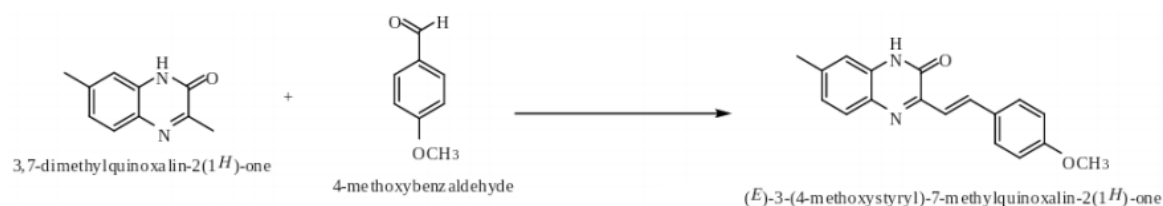
Corrosion tests have been carried out on electrodes cut from sheets of C35 steel. Steel strips containing 0.36 wt.% C, 0.66 wt.% Mn, 0.27 wt.% Si, 0.02 wt.% S, 0.015 wt.% P, 0.21 wt.% Cr, 0.02 wt.% Mo, 0.22 wt.% Cu, 0.06 wt.% Al and the rest iron. The working area of 1 cm^2 was subsequently ground with 180 and 1200 grit grinding papers, cleaned by distilled water and ethanol at hot air. The effect of temperature on the inhibition efficiencies for all inhibitors were tested between 303 -333 K.

2.2. Synthesis

Studied inhibitors are synthesized in our laboratory according to the procedure described in the schemes 1 and 2. In the literature, 3,7-dimethylquinoxalin-2-one is prepared following to Philip's method [20-22](scheme 1). The bibliography reports various methods to prepare styrylquinoxalines [23,24]. For our part, we suggested a different synthetic route which comprises reacting fusion 3,7-dimethylquinoxalin-2-one with aromatic aldehydes. This method, carried out in the absence of solvent, we have a possibility to isolate the desired compound in a yield of around 85% (Scheme 2). Indeed, 5,74 mmol of 3,7-dimethylquinoxalin-2-one is used with 8,61 mmol of 4-methoxybenzaldehyde for 2 hours at the boiling temperature of the latter. At the end of the reaction, the solid compound is allowed to cool and then heated at 100°C for 10 minutes in 50 ml of ethanol. The product is filtered hot then washed with ethanol [25].

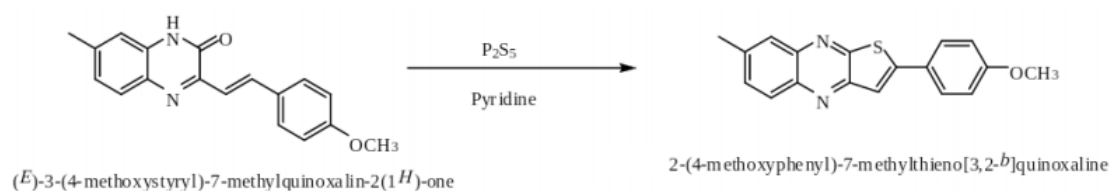


Scheme 1. Synthesis of 3,7-dimethylquinoxalin-2(1H)-one



Scheme 2. Synthesis of (E)-3-(4-methoxystyryl)-7-methylquinoxalin-2(1H)-one

2-(4-methoxyphenyl)-7-methylthieno[3,2-b]quinoxaline (TMQ) have been prepared by a new method developed in our laboratory :3,42mmol of (E)-3-(4-methoxystyryl)-7-methylquinoxalin-2(1H)-one (SMQ) undergoes sulfuration by P₂S₅, 84mmol, for 10h at reflux of pyridine. After evaporating the solvent to dryness, the product is recrystallized in ethanol (Scheme 3).



Scheme 3. Synthesis of 2-(4-methoxyphenyl)-7-methylthieno[3,2-b]quinoxaline

2.3. Electrochemical measurements

Electrochemical measurements, including stationary methods (PDP) and transient (EIS) were performed in a three-electrode cell. Pure C35 steel specimen was used as the working electrode, a saturated calomel (SCE) as reference and an area platinum as counter electrode (CE) were used. All potentials were measured against EC. The working electrode was immersed in a test solution for 30 min until the corrosion potential of the equilibrium state (E_{corr}) was achieved using a type PGZ100 potentiostat. The potentiodynamic polarization curves were determined by a constant sweep rate of 1 mV/ s. The measurements of the transitory method (EIS) were determined, using ac signals of amplitude 10 mV peak to peak at different conditions in the frequency range of 100 kHz to 10 mHz. The data obtained by PDP and EIS methods were analyzed and fitted using graphing and analyzing impedance software, version Zview 2. The inhibition efficiency of the studied compounds was calculated using the following equation:

$$\eta = \frac{i_{\text{corr}}^{\circ} - i_{\text{corr}}}{i_{\text{corr}}^{\circ}} \times 100$$

where i_{corr} and i_{corr}° are the corrosion rates in the presence and absence of inhibitors, respectively. The impedance diagrams were determined by EIS method. To confirm reproductibility, all experiments were repeated three times and the evaluated inaccuracy does not exceed 10%. The inhibition efficiency was calculated using the following equation:

$$\eta = \frac{R_p - R_p^0}{R_p} \times 100$$

where R_p^0 and R_p are the polarization resistance values without and with inhibitors, respectively.

2.4. Theoretical and Monte Carlo simulation details

All quantum chemical calculations of quinoxaline derivatives were performed at the DFT using B3LYP, CAM-B3LYB and B3PW91 at 6-31G (d, p) basis sets implemented in Gaussian03 program[26–29]. The adsorption configuration of TMQ and SMQ on iron surface were dynamically simulated by using the Materials Studio 6.0 software from Accelrys Inc[30]. The Fe crystal was chosen to represent the CS surface. First the crystal was cleaved along the (1 1 0) plane, as it is the most stable surface as reported in the literature [31]. Then, the Fe (1 1 0) plane was subsequently enlarged into an appropriate supercell to provide a large surface for the interaction of the inhibitor. The interaction between TMQ, SMQ and Fe surface was assumed in a simulation box ($29.78 \times 29.78 \times 60.13 \text{ \AA}$) with periodic boundary conditions. After that, thickness of the vacuum slab was 50 \AA . COMPASS force field was chosen to optimize the structures of all components of the system of interest. More detail of MC simulation is referenced from the published articles[31,32].

3. Results and discussion

3.1. Polarization measurements

The effect of SMQ, and TMQ was studied using potentiodynamic polarization curves. Fig. 1 shows the obtained results of carbon steel in 1M HCl in the absence and presence of each compound at different concentrations.

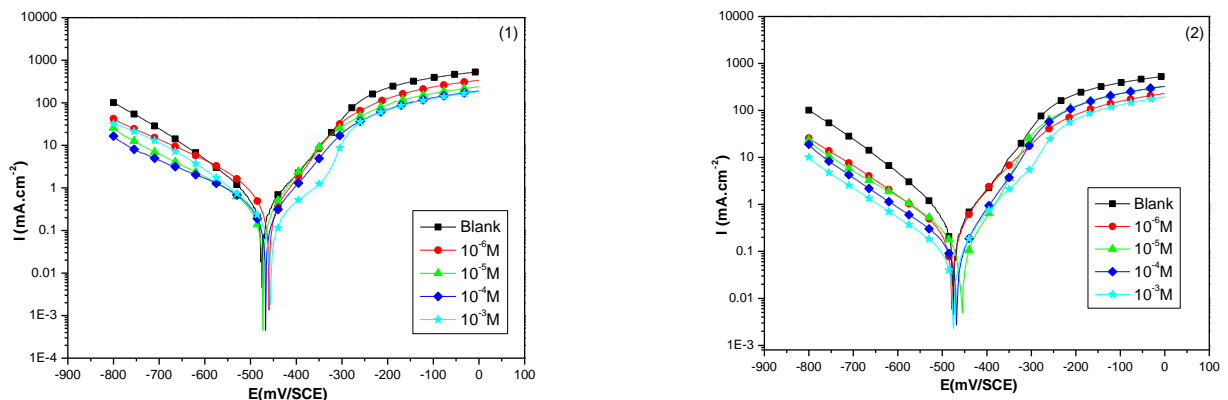


Figure 1: Potentiodynamic polarization curves for carbon steel at 303 K in 1M HCl solution in the absence and the presence of SMQ (1) and TMQ(2) at various concentrations.

The figure 1 shows polarization curves for carbon steel at 303 K in 1 M HCl with and without different concentration of SMQ (1) and TMQ (2). The polarization curves show the reactions of the anodic dissolution of the metallic surface and the cathodic hydrogen evolution reaction was slowed with and without of test compounds in different concentrations. Generally, the organic inhibitors acted by physical or chemical adsorption or both on the surface of the metal. The slowdown of reactions anodic and cathodic is marked with rise of concentration inhibitors.

The compounds tested, are reacted by adsorption onto the carbon steel surface, causing blockage of reaction sites. The addition of the inhibitor in hydrochloric acid causes a slight displacement of the corrosion potential (see fig 1). In literature, it has been also reported that if the displacement in E_{corr} in presence of inhibitor compared with E_{corr}^0 uninhibited solution is greater than 85 mV, the inhibitor can be considered as an anode or cathode type inhibitor, and if it is less than 85 mV, the inhibitor can be considered as mixed type [33]. From this data, the maximum displacement of E_{corr} values was 17.5mV for SMQ and 17.2mV for TMQ, indicating that these inhibitors act as an inhibitor of mixed type [34-36].

The kinetic parameters values, such as, corrosion current density (I_{corr}), Tafel slopes anodic and cathodic (β_a, β_c), corrosion potential (E_{corr}), degree of surface coverage (θ) derived are represented in Table 1.

From Table 2 it is observed that the corrosion current density (I_{corr}) decreases with addition of various concentrations of inhibitors. the presence of the inhibitors (SMQ and TMQ) slightly changes cathodic Tafel slope (β_c), which suggests that the inhibiting action is made by simple blocking of the available necessary for hydrogen evolution and lowered cathodic sites on the metal surface, which cause a decrease in the exposed area the dissolution rate with increasing SMQ concentration[37,38]. The parallel cathodic Tafel plots obtained in Fig. 1 show that hydrogen evolution is controlled by the activation and the presence of the inhibitor has no influence on the reduction mechanism[39].

Table 2. kinetic parameters calculated from PDP measurements after 30min of immersion in 1M HCl solution with and without inhibitor concentrations at 303K.

Inhibitor	Concentration (M)	E_{corr} (mV/SCE)	I_{corr} (mA cm ⁻²)	β_a (mV dec ⁻¹)	$-\beta_c$ (mV dec ⁻¹)	η (%)
Blank	1	-477	0.583	101.4	137.8	-
SMQ	10 ⁻⁶	-463.8	0.234	70.7	84.5	60
	10 ⁻⁵	-477.7	0.155	64.1	99.0	73
	10 ⁻⁴	-471.4	0.117	64.8	84.6	80
	10 ⁻³	-459.5	0.056	44.1	55.3	90
TMQ	10 ⁻⁶	-483.1	0.127	61.8	99.3	78
	10 ⁻⁵	-459.8	0.079	66.6	92.7	86
	10 ⁻⁴	-471.9	0.059	58.2	97.8	90
	10 ⁻³	-479.2	0.042	59.9	102.9	93

The inhibition efficiency calculated from the I_{corr} values obtained in the absence and presence of SMQ and TMQ varied from 93 to 60 % over a concentration range of 10⁻³-10⁻⁶ M.

3.2. Electrochemical impedance spectroscopy (EIS) study:

The results obtained by the PDP technique are insufficient to characterize complex mechanisms. The use of EIS technique is essential. Fig. 2 shows the Nyquist plots acquired at the open-circuit potential after 30 min of immersion. When analyzing the Nyquist diagrams, we show that these curves consist of a depressed capacitive loop semicircle with one capacitive time constant in Bode-phase plots for all compounds study, illustrated in Fig. 4a and 4b.

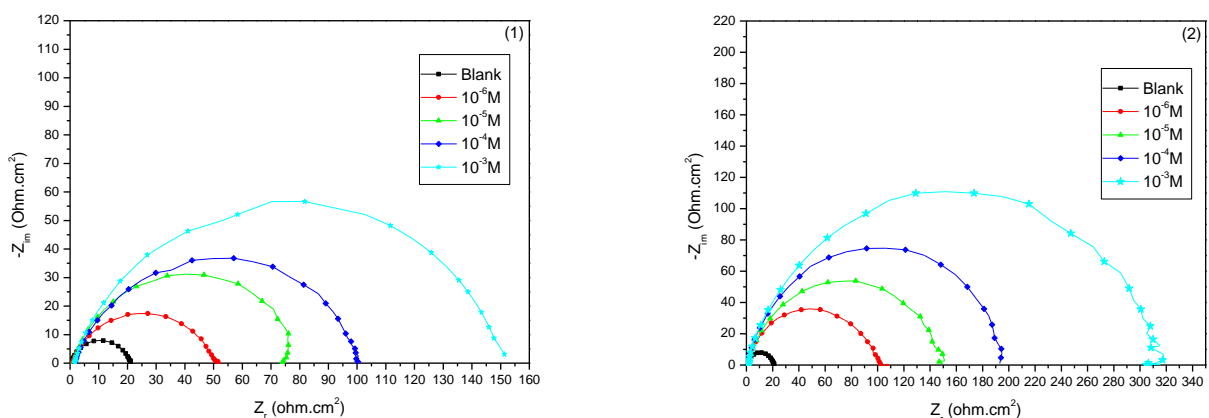


Figure 2: Nyquist plots for carbon steel at 303 K in 1 M HCl in various concentrations of the studied inhibitors: (1) SMQ, (2) TMQ

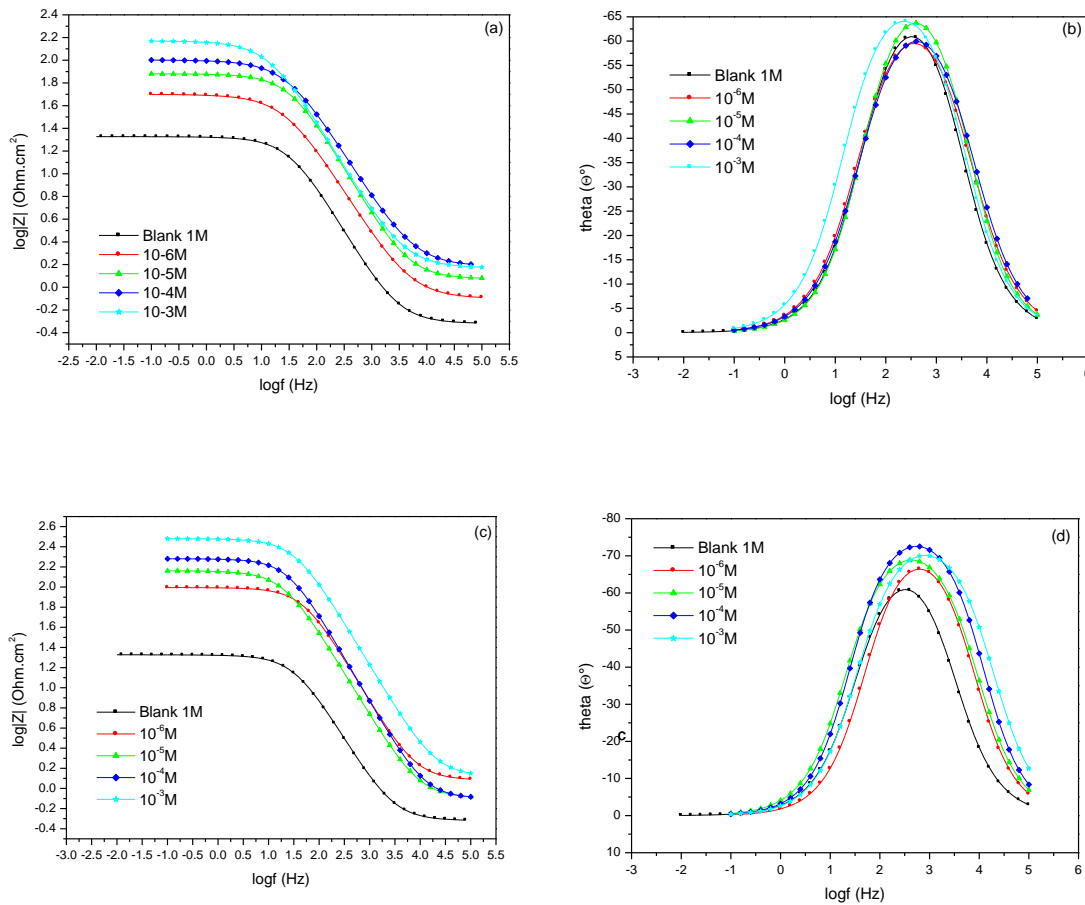


Figure 3: The Bode and phase angle plots for carbon steel in 1M HCl in the absence and presence of different concentrations of inhibitors 303 K, along with an immersion time of 30min: (a and b) SMQ, (c and d) TMQ.

The form of the capacitive loops shows that the corrosion process was controlled by charge transfer. We noted that the obtained impedance responses were significantly changed by addition of different concentration of inhibitor. The diameter of these capacitive loops increases gradually with rise of inhibitors concentration of SMQ and TMQ, indicating strengthening of inhibitive film. The Nyquist plots are evaluated in terms of the equivalent circuit composed with a constant phase element (CPE).

The capacitive loops obtained in absence and presences of inhibitors are not perfect semicircles due a frequency dispersion which has been attributed to the surface heterogeneity.

The main parameters (R_s , R_{ct} , Q and n) extracted from the Nyquist diagram to 1 M HCl with and without various concentrations of SMQ and TMQ are given in Table 3. The estimated margins of error for calculated parameters are also shown in table 3.

The CPE impedance is defined by two values, Q and n and is described by the equation [40, 41]:

$$Z_{CPE} = Q^{-1} \cdot (i\omega)^{-\alpha}$$

Where Q is the CPE constant, ω is the angular frequency (in rad.s^{-1}), such as $i^2 = -1$ is the imaginary number and n is a CPE exponent which can be employed as a gauge of the heterogeneity or roughness of the surface [42,43]. The CPE compartment can be quantified by plotting the imaginary part of the impedance as a versus frequency in logarithmic coordinates. The parameters associated with Nyquist plots (C_{dl} , R_{ct} , n , Q and $\%E$) were determined by the equivalent circuit presented in Fig. 4. This circuit gives an exact fit to all experimental impedance data for our inhibitors. The equivalent circuit is composed of charge transfer resistance (R_{ct}),

constant phase angle (CPE) and a solution resistance (R_s). The regression results are regrouped in Table 3. The double layer capacitance values (C_{dl}) presented in the same table were calculated via equation[44, 46]:

$$C_{dl} = (Q \times R_{ct}^{1-\alpha})^{1/\alpha}$$

Table 3. Electrochemical impedance measurements for carbon steel immersed in 1M HCl for 30min in the absence and presence at different concentrations of inhibitors.

	Conc (M)	$R_s(\Omega \text{ cm}^2)$	$R_{ct}(\Omega \text{ cm}^2)$	$10^4 Q(\Omega^{-1} \text{ cm}^{-2} \text{ s}^{-n})$	n	$C_{dl}(\mu\text{F cm}^{-2})$	$\tau(\text{F } \Omega)$	$\eta(\%)$
Blank	1M	0.54±0.02	20.27±0.44	4.65±0.05	0.804	149.15	3.02E-3	-
SMQ	10 ⁻⁶	0.87±0.02	48.37±0.73	3± 0.02	0.830	126.06	6.10E-3	59
	10 ⁻⁵	1.23±0.02	76.02±1.28	2.4± 0.08	0.860	125.06	9.51E-3	73
	10 ⁻⁴	1.51±0.02	98.87±1.03	1.45±0.06	0.882	82.17	8.12E-3	79
	10 ⁻³	1.50±0.02	149.7±2.58	1.25±0.09	0.889	76.06	1.13E-2	87
TMQ	10 ⁻⁶	1.20±0.03	97.67±1.16	2.76±0.04	0.812	119.55	1.17E-2	79
	10 ⁻⁵	0.87±0.03	142.4±2.98	1.07±0.07	0.851	51.43	7.32E-3	86
	10 ⁻⁴	0.88±0.03	187.5±3.94	0.78 ±0.04	0.852	42.32	7.93E-3	89
	10 ⁻³	1.37±0.03	299.8±4.55	0.32±0.02	0.890	18.01	2.40E-3	94

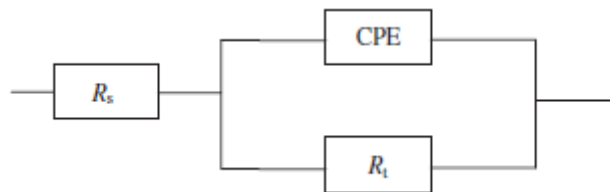


Figure4: The equivalent circuit model of EIS

The relaxation time constants were calculated by the equation [47, 48]:

$$\tau = C_{dl} \times R_{ct}$$

The results of Table 2 show that the charge transfer resistance (R_{ct}) and efficiency (%E) increase with augmentation of inhibitors concentration. However, the value of double layer capacitance (C_{dl}) decrease because it's depends inversely of charge transfer resistance in all concentration. This results may be attributed to the formation of a protective layer on the electrode surface [49].

The values of surface heterogeneity were exponent n ($0 \leq n \leq 1$) [50]. This parameter increases with increasing of the inhibitor concentration and it varied between 0.804 and 0.889. This increase can be attributed to the reduction of surface heterogeneity due to the adsorption of inhibitor compounds on the maximum active sites on the metal surface.

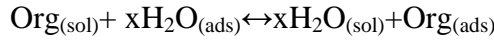
The time constants τ increase with increasing of concentration. The values of τ in uninhibited acidic solutions are less than in the inhibited solution. The results show that the SMQ and TMQ inhibit the corrosion of carbon steel in 1 M HCl solution at different concentration studied and the efficiency increase with rise of concentration at 303 K (table 3). The IE(%) obtained from EIS techniques and those calculated from polarization curves measurements are in good agreements in all compounds.

3.3. Thermodynamic parameters of the adsorption process

3.3.1. Adsorption isotherm

The organic corrosion inhibitor reacts in acidic media by adsorption the metal/solution interface. The adsorption depends essentially on the structures and electronic properties of inhibitor compounds, such as, aromaticity,

electronic density on donor atom and the π orbital character of donating electrons [51,52]. Furthermore, the solvent H_2O molecules can be adsorbed at the metal/solution interface. Therefore, the adsorption of organic inhibitor compounds from the aqueous solution can be considered as a quasi-substitution process between the organic molecules in the aqueous phase $Org_{(sol)}$ and water molecules at the electrode surface $H_2O_{(ads)}$ [53]:



Where x is the size ratio, that is, the number of water molecules changed by one organic inhibitor. The adsorption isotherm can be giving information about the properties of the tested inhibitors. The degree of surface coverage (θ) of the inhibitor is calculated, for determine the adsorption isotherm. In this study, degree of surface coverage values (θ) for the concentrations of inhibitors range between $10^{-3}M$ and $10^{-6}M$ in acidic media have been determined from the PDP measurements and regrouped in Table 4. For defined the mode of adsorption isotherm, different fit of the θ values to various isotherms, as well as, Temkin, Langmuir, Frumkin and Flory-Huggins, were made. The excellent fit is obtained with the Langmuir isotherm. Langmuir adsorption isotherm is described by the following equations:

$$\frac{\theta}{1 - \theta} = K_{ads} C_{inh}$$

By rearranging this equation :

$$\frac{C_{inh}}{\theta} = \frac{1}{K_{ads}} + C_{inh}$$

Where K_{ads} is the adsorption equilibrium constant, C_{inh} is the inhibitor concentration, and θ is the surface coverage. Fig. 5 shows the plots of C_{inh}/θ versus C_{inh} and the estimated linear correlation is obtained for SMQ and TMQ.

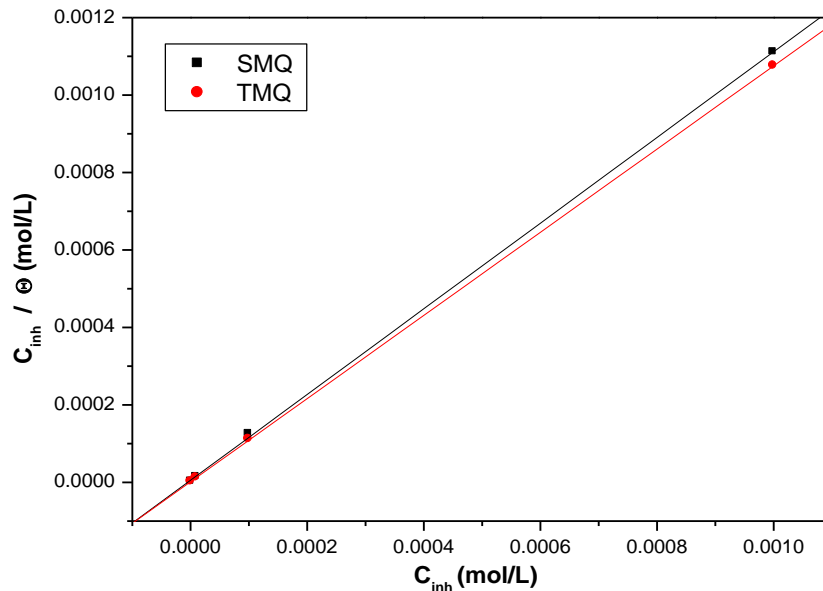


Figure 5: Langmuir adsorption isotherm plot for carbon steel in 1M HCl at different concentrations of the studied inhibitors.

The strong correlations ($R^2=0.99994$ and $R^2=0.99998$) confirm the validity of this approach. The adsorption equilibrium constant (K_{ads}) has been found to be $0.1843E5M^{-1}$ for SMQ and $0.653E6 M^{-1}$ for TMQ (Table 4)

suggesting that the adsorbed inhibitor molecules form monolayer on the carbon steel surface and there is no interaction among the adsorbed inhibitor molecules [54]. On the other hand, the high value of adsorption equilibrium constant reflects the high adsorption capacity of SMQ and TMQ on carbon steel surface [55,56]. The standard free energy of adsorption (ΔG_{ads}°) can be determined by the following equation:

$$\Delta G_{ads}^{\circ} = -RT \ln(55.5 K_{ads})$$

where R is the gas constant ($8.314 \text{ J K}^{-1} \text{ mol}^{-1}$), T is the absolute temperature (K), the value 55.5 is the concentration of water in solution expressed in M[57].

Table 4. Thermodynamic parameters for the adsorption of SMQ and TMQ in 1.0 M HCl on the C-steel at 303 K

Inhibitors	$K_{ads} (M^{-1})$	$-\Delta G_{ads}^{\circ} (KJ.mol^{-1})$	R^2
SMQ	0.1844E5	34.861	0.99994
TMQ	0.2915E5	36.015	0.99998

The ΔG_{ads}° value is calculated as $-34.861 \text{ kJ mol}^{-1}$ for SMQ and $-36.015 \text{ kJ mol}^{-1}$ for TMQ. In the literature, if the absolute values of ΔG_{ads}° are less than 20 kJ mol^{-1} consistent with the electrostatic interaction between the charged metal and charged molecules (physisorption), but if those more than 40 kJ mol^{-1} involve sharing or transfer of electrons from the inhibitor compound to the metal surface to form a co-ordinate type of bond (chemisorption) [58,59]. The values of ΔG_{ads}° calculated in this study are between 20 kJ mol^{-1} and 40 kJ mol^{-1} suggest that the adsorption of our inhibitors has the type of interactions: physisorption and chemisorption [60].

3.3.2. Effect of temperature

The impact of temperature on the corrosion inhibition is studied using the PDP measurement, in the range of 303–333 K, without and with 10^{-3} M of SMQ and TMQ during 30 min of immersion. The analysis of the obtained data, included in Table 5 and presented in Fig 6. (a, b and c) shows an increase of I_{corr} with increasing of temperature and it is more pronounced for uninhibited solution.

We note a slight variation in the inhibitor efficiency with the rise of temperature, indicating that the higher temperature does not influence on the adsorption of SMQ and TMQ on the metal surface.

Table 5. Temperature influence on the PDP parameters for carbon steel in 1 M HCl with and without HCl (1M)+ 10^{-3} M of SMQ and HCl (1M)+ 10^{-3} M of TMQ at range temperature 303K-333K.

Inhibitor	Temperature (K)	E_{corr} (mV/SCE)	I_{corr} (mA cm^{-2})	β_a (mV dec^{-1})	$-\beta_c$ (mV dec^{-1})	$\eta(\%)$	θ
Blank	303	-477	0.583	101.4	137.8	-	-
	313	-457.7	0.781	78.7	88.1	-	-
	323	-447.5	0.882	53.5	47.6	-	-
	333	455.1	0.999	18.6	31.7	-	-
SMQ	303	-459.5	0.056	44.1	55.3	90	0.90
	313	-457.7	0.148	66.2	92.7	81	0.81
	323	-457.8	0.259	67.7	86.8	71	0.71
	333	-474.3	0.367	37.9	39.7	63	0.63
TMQ	303	-479.2	0.042	59.9	102.9	93	0.93
	313	-486.4	0.075	64.1	81.4	90	0.90
	323	-495.3	0.129	29.7	35	85	0.85
	333	-491	0.179	36.1	41.7	82	0.82

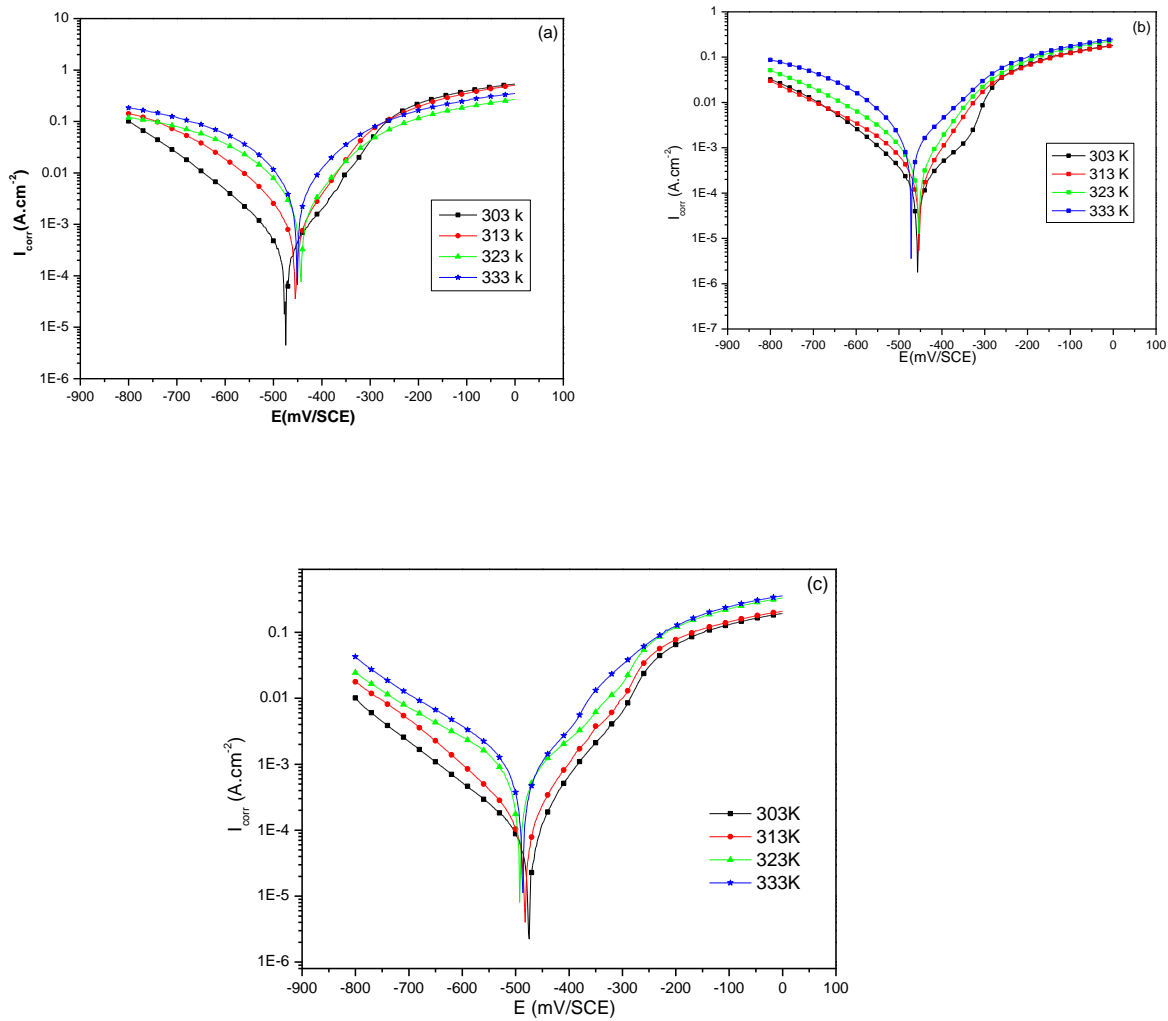


Figure 6: Effect of temperature on the behaviour of carbon steel/1M HCl interface in (a) uninhibited solution, (b) at 10^{-3} M of SMQ and (c) 10^{-3} M of TMQ.

3.3.3. Activation parameters

The activation thermodynamic parameters of the corrosion process, Arrhenius Eq. and Eq. transition state were calculated using [61]:

$$i_{corr} = A \exp\left(-\frac{E_a}{RT}\right)$$

$$i_{corr} = \frac{RT}{Nh} \exp\left(\frac{\Delta S_a}{R}\right) \exp\left(-\frac{\Delta H_a}{RT}\right)$$

Where E_a is the apparent activation corrosion energy, R is the universal gas constant, A is the Arrhenius pre-exponential factor, h is Planck's constant, N is Avogadro's number, ΔS_a is the entropy of activation and ΔH_a is the enthalpy of activation.

Arrhenius plots for the corrosion rate of carbon steel are given in Fig.7. Using the slope of $\ln(i_{corr})$ vs. $1/T$ plots, it has been determined the values of the apparent activation energy of corrosion (E_a) (Table 5). The linear regression coefficient was close to 1, showing that the corrosion of carbon steel in chlorhydrique acid 1M can be interpreted using the kinetic model. The value calculated of E_a uninhibited solution ($19.12 \text{ kJ mol}^{-1}$) is in the same order of magnitude as previously described [62-64]. The obtained E_a values in the presence SMQ and TMQ are respectively $52.38 \text{ kJ mol}^{-1}$ and $42.06 \text{ kJ mol}^{-1}$. E_a value in the absence of the inhibitor is less than that

in its presence can be explained as a physical adsorption [65]. The increase in activation energy may be due to desorption of the inhibitor on the surface of the steel with increasing temperature [66]. Fig. 8 shows a plot of $\ln(i_{corr}/T)$ against $1/T$. A straight lines obtained with a slope of $(\Delta H_a/R)$ and an intercept of $(\ln R/Nh + \Delta S_a/R)$ from which the values of ΔH_a and ΔS_a are calculated and listed in Table 5. These data show that the ΔH_a value for dissolution reaction of carbon steel is higher in the presence of SMQ and TMQ (49.67 kJmol^{-1} and 38.49 kJmol^{-1}) than that in its absence (14 kJmol^{-1}). The positive signs of ΔH_a indicate the endothermic nature of the carbon steel dissolution process suggesting that its dissolution is slow in the presence of SMQ and TMQ[67].

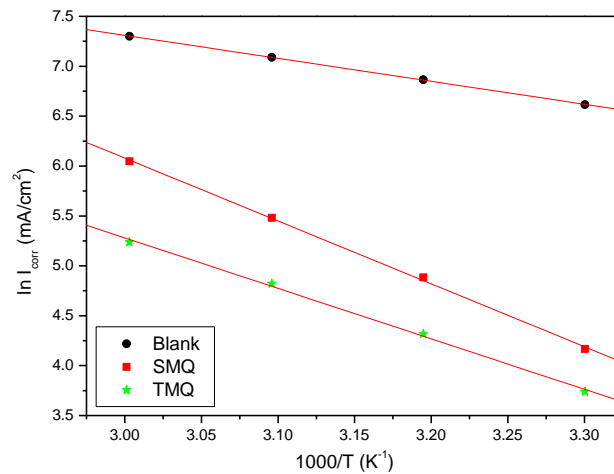


Figure 7: Arrhenius plots for carbon steel in 1 M HCl in absence and in presence of 10^{-3} M of SMQ and TMQ.

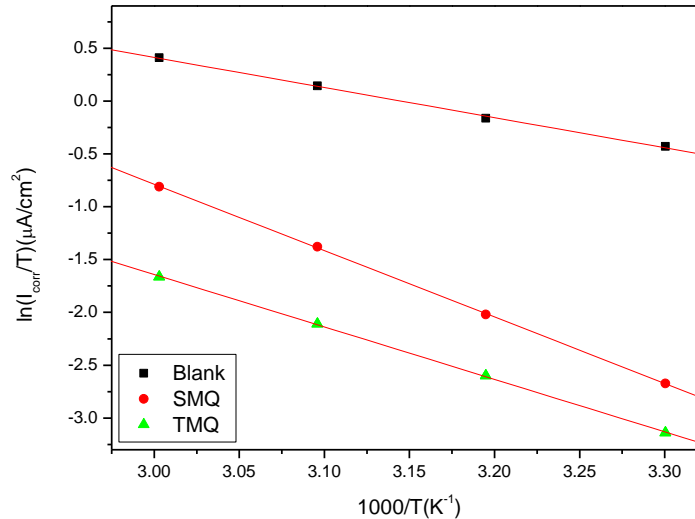


Figure 8: Transition-state plots for C-steel in 1 M HCl in absence and presence of 10^{-3} M of SMQ and TMQ

Table 6. Corrosion kinetic parameters for carbon steel in 1 M HCl in absence and presence of 10^{-3} M of SMQ and TMQ.

Inhibitor	E_a (KJ.mol ⁻¹)	Linear regression coefficient (R)	ΔH (KJ.mol ⁻¹)	ΔS (J.mol ⁻¹ .K ⁻¹)
Blank	19.12	0.9999	14	-208
SMQ	52.38	0.998	49.67	-104
TMQ	42.06	0.9992	38.49	-144.16

The increase of ΔS_a is usually interpreted as an increase in disorder as the reactants are converted to the activated complexes [68]. From Table 5, we note that a less negative value of ΔS_a is obtained in the presence of SMQ and TMQ, while a more negative value is observed in uninhibited solution. The values of ΔS_a calculated in presence of inhibitors decrease compared with blank solution. This result interpreted as an increase in disorder [69].

3.4. Quantum chemical calculations:

3.4.1. Global reactivity descriptors:

In order to explain the experimental findings and to search possible correlation between experimental results and electronic properties of tested compounds, the theoretical calculations by *DFT* method with three level, *B3LYB*, *CAM-B3LYB* and *B3PW91* at 6-31G (d, p) basis set were carried out. The optimized molecular structure of TMQ and SMQ are presented in Figure 9. The QCPs (Quantum chemical parameters) such as E_{HOMO} , E_{LUMO} , $\Delta E = (E_{LUMO} - E_{HOMO})$, softness (σ), the fraction of electrons transferred (ΔN) and dipole moment (μ) were collected in Table 7. The *IE* % of TMQ and SMQ according to our experimental studies is:

$$TMQ > SMQ$$

In Figure 9, The *HOMO* and *LUMO* orbitals are distributed over the entire quinoxaline molecules in all used methods, resulting in the highest interaction of inhibitors on the carbon steel surface. This observation also suggests that the heteroatoms and the cycle rings containing π -bonds are the probable reactive sites for adsorption of inhibitors on the metal surface. E_{HOMO} is a quantum chemical parameter which is associated with electron donating ability of the molecule; this ability becomes more considerable with a high value of E_{HOMO} and E_{LUMO} indicates the ability of the molecule to accept electrons [70,71]. The $\Delta E = (E_{LUMO} - E_{HOMO})$ was reported as a main chemical reactivity factor of an inhibitor from theoretical point of view [71]. According to these literature findings and the results from Table 7, it can be observed that the quinoxaline derivatives have higher interactions with the steel surface. Based on the results obtained in all used methods, the reactivity of TMQ and SMQ can be classified by the following order:

$$BMQ > FVQ > STQ$$

The absolute electronegativity (χ) and global hardness (η) of the inhibitors molecule are approximated as follows [72,73]:

$$\chi = \frac{I + A}{2}$$

$$\eta = \frac{I - A}{2}$$

Where: $I = -E_{HOMO}$ and $A = -E_{LUMO}$

Table 7. Calculated quantum chemical parameters of the inhibitors molecules

Model	Molecule	E_{HOMO} (eV)	E_{LUMO} (eV)	ΔE (eV)	μ (D)	η (eV)	σ (eV ⁻¹)	χ (eV)	ΔN
B3PW91	TMQ	-5.36	-2.14	3.21	2.88	1.60	0.62	3.75	0.33
	SMQ	-5.76	-2.23	3.53	1.99	1.76	0.56	3.99	0.23
B3LYB	TMQ	-5.25	-2.04	3.21	2.88	1.60	0.62	3.64	0.36
	SMQ	-5.65	-2.12	3.53	1.94	1.76	0.56	3.89	0.26
CAM-B3LYB	TMQ	-6.53	-0.84	5.68	3.06	2.84	0.35	3.68	0.20
	SMQ	-6.93	-0.97	5.95	1.65	2.97	0.33	3.95	0.14

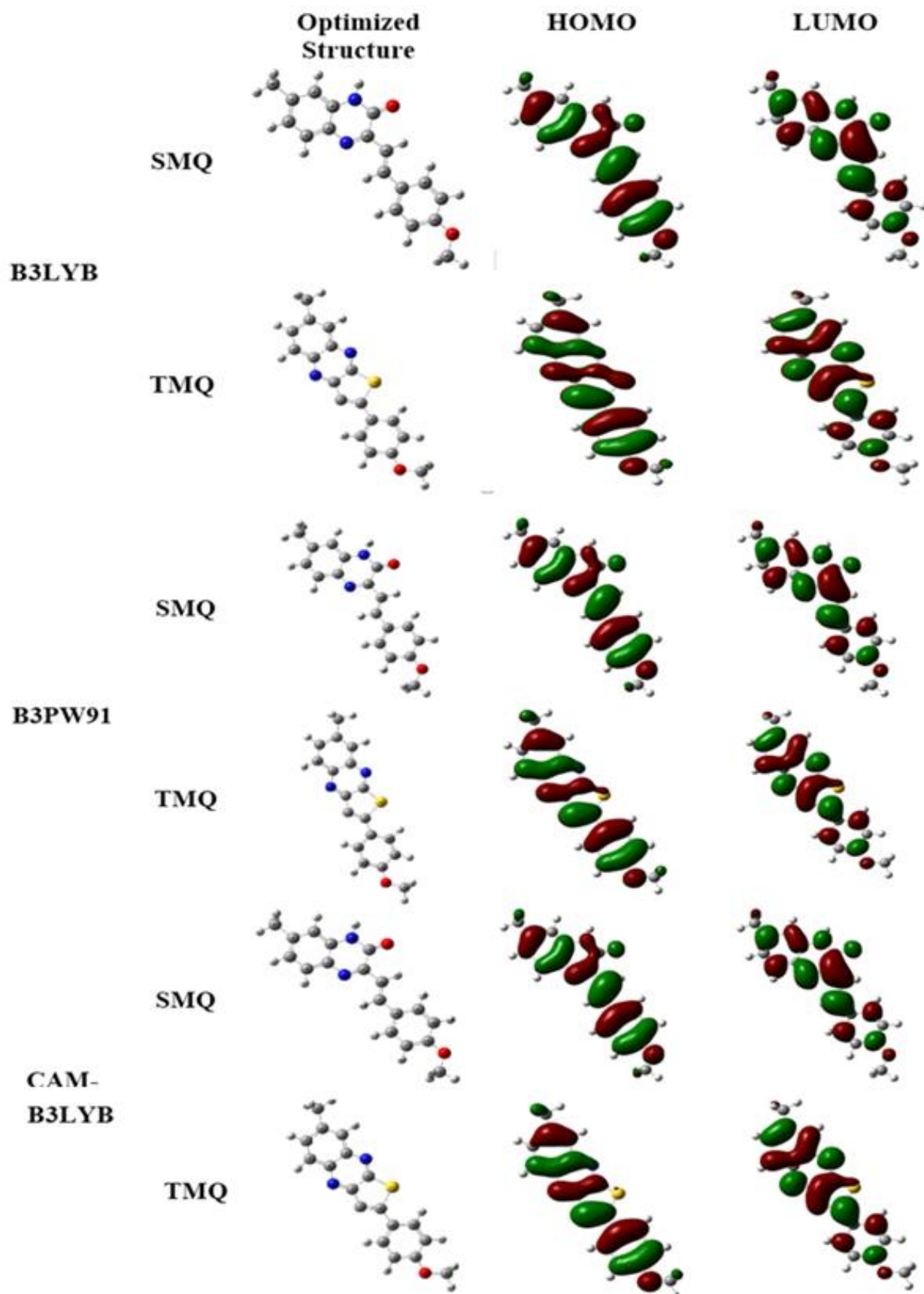


Figure9: Frontier molecule orbital density distributions of the synthesized inhibitors.

Thus the fraction of electrons transferred from the inhibitor to metallic surface, ΔN , is given by[74]:

$$\Delta N = \frac{\chi_{Fe} - \chi_{inh}}{2(\eta_{Fe} + \eta_{inh})}$$

The theoretical values of χ_{Fe} (4.06 eV mol⁻¹) and of η_{Fe} (0 eV mol⁻¹) are used to calculate ΔN [73,75]. The results from Table 7, show that the order of electron transfer in all basis set is such that TMQ>SMQ which also confirms that TMQ has the highest tendency to donate electrons and therefore the highest tendency to bind onto the metal surface[76,77].

3.4.2. Fukui Function

The nucleophilic/electrophilic sites (susceptible atoms and regions) in the molecular structures of quinoxaline derivatives were localized by the Fukui function[78,79]. The condensed Fukui functions were found by taking the finite difference approximations from the population analysis of atoms in molecules, depending on the direction of the electron transfer. The equations used for electrophilic attack and nucleophilic attack were eq. (4) and (6), respectively[80,81]:

$$f_k^+ = P_k(N + 1) - P_k(N)$$

$$f_k^- = P_k(N) - P_k(N - 1)$$

where $P_k(N + 1)$, $P_k(N)$, $P_k(N - 1)$ represent charge values of atom k for anion, neutral, and cation, respectively.

Generally, the high value of f_k^+ is the preferred site for nucleophilic attack, while the sites with a high value of f_k^- are preferred for electrophilic attack[81], The Fukui indices for TMQ and SMQ are present in Tables 8. In TMQ atoms N7 (0.043), C8 (0.050) and N10 (0.102), in SMQ atoms C9 (0.060), N10 (0.073) and C13 (0.064), presented the highest values of f_k^+ regarding the most susceptible sites for nucleophilic attacks. On the other hand, in TMQ atoms C8 (0.048), N10 (0.101) and C13 (0.040) and in SMQ atoms C12 (0.050), N10 (0.046) and O20 (0.050) are the preferable sites for electrophilic attacks and consequently donating charges to the CS surface, as they presented the highest values of f_k^- . Based on these findings, the distribution of the active sites is quite different. This implies the highest capacity of adsorption of our inhibitors on the CS surface; these results further confirm the experimental *IE* %.

3.5. Monte Carlo simulations

Nowadays, molecular dynamics simulation has been extensively used to describe the interactions between the inhibitor and metal surface, which gives a view of the motion of the atoms after interaction at a certain time[82,83]. Figure 10 represents the top and side views of the most suitable configuration for adsorption of quinoxaline derivatives on Fe (1 1 0) substrates obtained by Monte Carlo simulation. The outputs and descriptors calculated by the Monte Carlo simulation, such as the total adsorption, adsorption energy, rigid adsorption and deformation energies are presented in Table 9. Generally, the adsorption energy is defined as the sum of rigid adsorption energy and the deformation energy for the adsorbate components (quinoxaline derivatives). Whereas, the rigid adsorption energy is the energy in kcal/mol which is either released or absorbed when the unrelaxed quinoxaline molecules adsorbed on the Fe (1 1 0) surface. The deformation energy is the energy (in kcal/mol) released when the adsorbed adsorbate components are relaxed on the Fe (1 1 0) surface. The quantity (dE_{ads}/dNi) depicted in Table 9 represents the energy of Fe (1 1 0)-adsorbate configurations where one of the adsorbate components has been removed[84,85]. It is clearly observed from Figure 10 that the inhibitors adsorbed very nearly and in parallel to the Fe (1 1 0) surface in so, as to maximize surface contact. This adsorption process occurs mainly through the formation of the insoluble film on the Fe (1 1 0) surface. It is generally noted that the adsorption process is the primary mechanism of corrosion inhibitor interaction with the carbon steel. According to Table 9, the adsorption energies of inhibitors on the Fe (1 1 0) surface increased in

the order $TMQ > SMQ$. Which is in good accordance with the order of the $IE\%$ obtained by experimental and theoretical studies.

Table 8. The Fukui indices of TMQ and SMQ, calculated by DFT at B3LYP basis set

Atom	SMQ		Atom	TMQ	
	f_k^-	f_k^+		f_k^-	f_k^+
C (1)	0.016	0.011	C (1)	0.013	0.015
C (2)	0.019	0.033	C (2)	0.037	0.036
C (3)	0.006	-0.005	C (3)	-0.003	-0.002
C (4)	0.026	0.025	C (4)	0.023	0.022
C (5)	0.012	0.018	C (5)	0.020	0.021
C (6)	0.023	0.030	C (6)	0.030	0.028
N (7)	0.011	0.020	N (7)	0.041	0.043
C (8)	0.014	0.021	C (8)	0.048	0.050
C (9)	0.007	0.060	C (9)	0.014	0.015
N (10)	0.046	0.073	N (10)	0.101	0.102
O (11)	0.038	0.052	O (11)	0.024	0.024
C (12)	0.050	-0.005	C (12)	0.024	0.022
C (13)	0.025	0.064	C (13)	0.040	0.040
C (14)	0.020	-0.015	C (14)	-0.010	-0.011
C (15)	0.014	0.019	C (15)	0.026	0.024
C (16)	0.024	0.010	C (16)	0.007	0.008
C (17)	0.035	0.036	C (17)	0.035	0.034
C (18)	0.023	0.008	C (18)	0.011	0.010
C (19)	0.024	0.025	C (19)	0.018	0.018
O (20)	0.050	0.025	O (20)	0.023	0.025
C (21)	-0.027	-0.021	C (21)	-0.018	-0.020
C (22)	-0.011	-0.014	C (22)	-0.015	-0.015
H (23)	0.041	0.048	H (23)	0.053	0.053
H (24)	0.034	0.043	H (24)	0.051	0.051
H (25)	0.036	0.044	H (25)	0.047	0.047
H (26)	0.029	0.038	H (26)	0.038	0.038
H (27)	0.041	0.039	H (27)	0.045	0.045
H (28)	0.035	0.034	H (28)	0.025	0.024
H (29)	0.033	0.022	H (29)	0.034	0.034
H (30)	0.047	0.037	H (30)	0.037	0.036
H (31)	0.045	0.036	H (31)	0.022	0.021
H (32)	0.042	0.030	H (32)	0.017	0.017
H (33)	0.028	0.019	H (33)	0.026	0.026
H (34)	0.036	0.027	H (34)	0.017	0.018
H (35)	0.028	0.019	H (35)	0.032	0.032
H (36)	0.027	0.031	H (36)	0.037	0.037
H (37)	0.029	0.034	H (37)	0.030	0.031
H (38)	0.024	0.028			

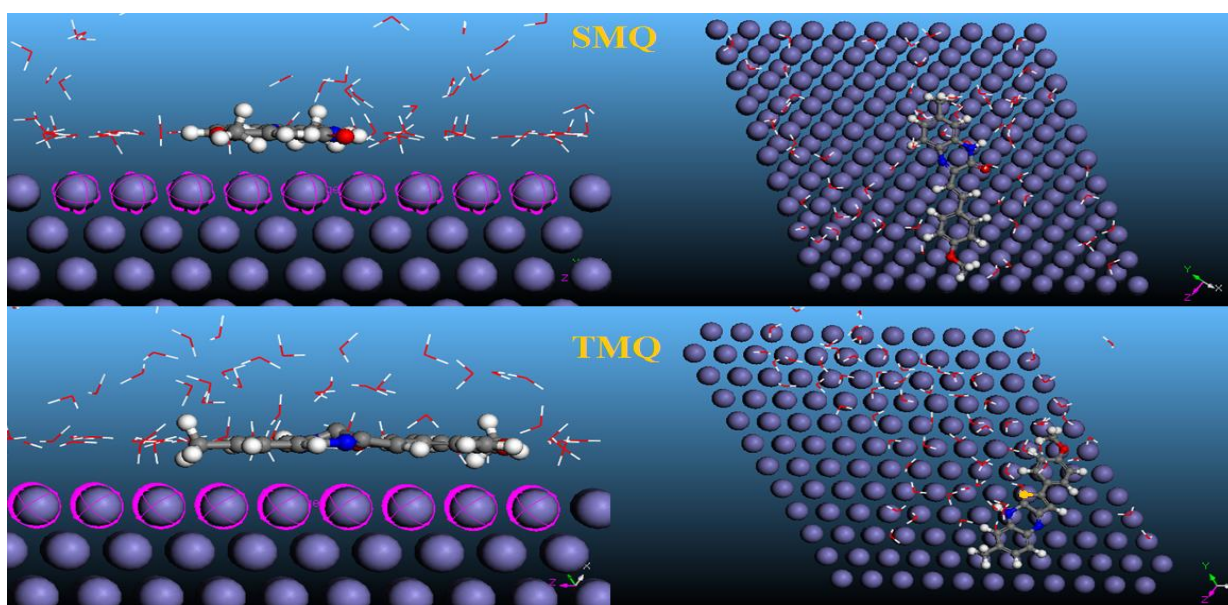


Figure 10: The side and top views of the most stable low energy configuration for the adsorption of the inhibitors on Fe (1 1 0)/100 H₂O surface obtained through the Monte Carlo simulation for SMQ and TMQ.

Table 9. Outputs and descriptors calculated by the Monte Carlo simulation for the lowest adsorption. Configurations of studied inhibitors Fe (110)/100 H₂O surface (in kcal/mol).

System	Total energy	Adsorption energy	Rigid adsorption energy	Deformation energy	dEad/dNi inhibitor	dEad/dNi Water
Fe (1 1 0)/TMQ/100 H ₂ O	-1464	-1506	-1556	50,95	-189,80	-6,276
Fe (1 1 0)/SMQ/100 H ₂ O	-1534	-1499	-1544	45,34	-205,18	-6,44

Conclusion:

The quinoxaline derivatives, namely (E)-3-(4-methoxystyryl)-7-methylquinoxalin-2(1H)-one (SMQ) and 2-(4-methoxyphenyl)-7-methylthieno[3,2-b]quinoxaline (TMQ) show good inhibitive properties for the corrosion of carbon steel in 1M HCl, with TMQ having higher performance than SMQ.

Comparing the methods used in this study, electrochemical impedance spectroscopy and potentiodynamic polarization; we note that there is a good according.

EIS measurements also show that the addition of inhibitor increases the charge transfer resistance and indicate that the inhibitive performance depends on molecules adsorption on the metal surface. The polarization measurements indicate that the inhibitor SMQ and TMQ are act as mixed type inhibitors. Inhibitory action is explained by the physical and chemical adsorption of SMQ and TMQ on the carbon steel surface and the adsorption process is a spontaneous endothermic process. The adsorption model of compounds obeys the Langmuir isotherm at 303 K. Quantum chemical calculation by DFT method and Monte Carlo simulations were performed to identify the reactivity of tested molecules towards corrosion inhibition, and the results are in good agreement with the experimental investigations. Both experimental and quantum chemical results showed that the order of inhibition efficiency, for the studied compounds is as follows: TMQ > SMQ.

References

1. Bentiss F., Gassama F., Barbry D., Gengembre L., Vezin H., Lagrene´e M., Traisnel M., *Appl. Surf. Sci.* 252 (2006) 2 684.
2. Khaled K.F., Hackerman N., *Electrochim. Acta.* 48 (2003) 2715.
3. Mihit M., El Issami S., Bouklah M., Bazzi L., Hammouti B., Ait Addi E., Salghi R., Kertit S., *Appl. Surf. Sci.* 252 (2006) 2389.

4. Hammouti B., Salghi R., Kertit S., *J. Electrochem. Soc. India.* 47 (1998) 31.
5. Zarrok H., Oudda H., Zarrouk A., Salghi R., Hammouti B., Bouachrine M., *Der Pharm. Chem.* 3(2011) 576
6. El Issami S., Bazzi L., Mihit M., Hilali M., Salghi R., Ait Addi El., *J. Phys. IV.* 123 (2005) 307.
7. El Issami S., Bazzi L., Mihit M., Hammouti B., Kertit S., Ait Addi E., Salghi R., *Pigm. Res. Techn.* 36 (2007) 161.
8. Mihit M., Laarej K., Abou El Makarim H., Bazzi L., Salghi R., Hammouti B., *Arabian J. Chem.* 3 (2010) 55.
9. Mihit M., Salghi R., El Issami S., Bazzi L., Hammouti B., Ait Addi E., Kertit S., *Pigm. Res. Techn.* 35 (2006) 151.
10. Barouni K., Bazzi L., Salghi R., Mihit M., Hammouti B., Albourine A., El Issami S., *Mater. Lett.* 62 (2008) 3325.
11. El Issami S., Bazzi L., Hilali M., Salghi R., Kertit S., *Ann. Chim. Sci. Mat.* 27 (2002) 63.
12. Salghi R., Bazzi L., Hammouti B., Kertit S., *Bull. Electrochem.* 16 (2000) 272.
13. Ben Hmamou D., Salghi R., Zarrouk A., Zarrok H., Hammouti B., Al-Deyab S.S., Bouachrine M., Chakir A., Zougagh M., *Int. J. Electrochem. Sci.* 7 (2012) 5716-5733
14. Zarrouk A., Hammouti B., Al-Deyab S.S., Salghi R., Zarrok H., Jama C., Bentiss F., *Int. J. Electrochem. Sci.* 7 (2012) 5997-6011
15. Zarrouk A., Zarrok H., Salghi R., Hammouti B., Al-Deyab S.S., Touzani R., Bouachrine M., Warad I., Hadda T. B., *Int. J. Electrochem. Sci.* 7 (2012) 6353 – 6364
16. Lashkari M., Arshadi M., *Chem. Phys.* 299 (2004) 131–137.
17. Verma C., Ebenso E., Bahadur I., Obot I., Quraishi M., *J. Mol. Liq.* 212 (2015) 209–218.
18. Al-Mobarak N., Khaled K., Hamed M.N., Abdel-Azim K., Abdelshafi N., *Arab. J. Chem.* 3 (2010) 233–242.
19. Yan Y., Wang X., Zhang Y., Wang P., Zhang J., *Mol. Simul.* 39 (2013) 1034–1041.
20. Landquis. J. K., Stacey G. J., *J. Chem. Soc.*, 1953, 2822.
21. Ramli Y., Moussaif A., karrouchi K., Essassi E. M., *Journal of Chemistry* (2014) Article ID 563406.
22. Lgaz H., ELaoufir Y., Ramli Y., Larouj M., Zarrok H., Salghi R., Zarrouk A., Elmidaoui A., Guenbour A., Essassi E. M., Oudda H., *Der Pharma Chemica*, 7(6) (2015)36.
23. Landquist J. K., Stacey G. J., *J. Chem. Soc.*, (1953), 2822.
24. Ried Hinsching W., Liebig Ann S., *Chem.*, (1956), 47, 600.
25. Adardour K., Tourir R., Ramli Y., Belakhmima R. A., Ebn Touhami M., Kalonji Mubengayi C., El Kafsaoui H., Essassi E. M., *Res. Chem. Intermed.*, 39 (4) (2013) 1843.
26. Becke A.D., *J. Chem. Phys.* 96 (1992) 2155–2160.
27. Becke A.D., *J. Chem. Phys.* 98 (1993) 5648–5652.
28. Lee C., Yang W., Parr R.G., *Phys. Rev. B.* 37 (1988) 785.
29. Frisch M., Trucks G., Schlegel H., Scuseria G., Robb M., Cheeseman J., Montgomery J. Jr., Vreven T., Kudin K., Burant J., *Gaussian 03, revision B. 05; Gaussian, Inc Pittsburgh PA.* (2003) 12478.
30. Materials Studio, Revision 6.0, Accelrys Inc., San Diego, USA, 2013.
31. Sasikumar Y., Adekunle A., Olasunkanmi L., Bahadur I., Baskar R., Kabanda M., Obot I., Ebenso E., *J. Mol. Liq.* 211 (2015) 105–118.
32. Eivani A., Zhou J., Duszczek J., *Comput. Mater. Sci.* 54 (2012) 370–377.
33. Satapathy A.K., Gunasekaran G., Sahoo S.C., Amit k., Rodrigues P.V., *Corros. Sci.* 51 (2009) 2848.
34. Deng Q., Shi H.W., Ding N.N., Chen B.Q., He X.P., Liu G., Tang Y., Long Y.T., Chen G.R., *Corros. Sci.* 57 (2012) 220.
35. Satapathy A.K., Gunasekaran G., Sahoo S.C., Amit K., Rodrigues P.V., *Corros. Sci.* 51 (2009) 2848.
36. John S., Joseph B., Aravindakshan K.K., Joseph A., *Mater. Chem. Phys.* 122 (2010) 374.
37. Tao Z., Zhang S., Li W., Hou B., *Corros. Sci.* 51 (2009) 2588
38. Pauline S.A., Sahila S., Gopalakrishnan C., Nanjundan S., Rajendran N., *Prog. Org. Coat.* 72 (2011) 443.
39. Bentiss F., Jama C., Mernari B., El Attari H., El Kadi L., Lebrini M., Traisnel M., Lagrenée M., *Corros. Sci.* 51 (2009) 1628
40. Stoynov Z., *Electrochim. Acta.* 35 (1990) 1493–1499.
41. Macdonald J.R., *J. Electroanal. Chem.* 223 (1987) 25–50.
42. Li P., Lin J.Y., Tan K.L., Lee J.Y., *Electrochim. Acta.* 42 (1997) 605–615.
43. Lopez D.A., Simison S.N., de Sanchez S.R., *Electrochim. Acta.* 48 (2003) 845–854
44. Martinez S., Metikos-Hukovic M., *J. Appl. Electrochem.* 33 (2003) 1137–1142.

45. Wu X., Ma H., Chen S., Xu Z., Sui A., *J. Electrochem. Soc.* 146 (1999) 1847–1853.
46. Ma H., Cheng X., Li G., Chen S., Quan Z., Zhao S., Niu L., *Corros. Sci.* 42 (2000)1669–1683.
47. Wu X., Ma H., Chen S., Xu Z., Sui A., *J. Electrochem. Soc.* 146 (1999) 1847 -1853.
48. Toshima S., Uchida T., *Electrochim. Acta.* 15 (1970) 1717-1732.
49. Lebrini M., Lagrenée M., Vezin H., Traisnel M., Bentiss F., *Corros. Sci.* 49 (2007) 2254–2269.
50. Lopez D.A., Simison S.N., de Sanchez S.R., *Electrochim. Acta*, 48 (2003) 845–854.
51. Quraishi M.A., Sharma H.K., *Chem. Phys.* 78 (2002) 18.
52. Quraishi M.A., SardarR., *Mater. Chem. Phys.* 78 (2002) 425.
53. Wang X., Yang H., Wang F., *Corros. Sci.*, 52 (2010) 1268.
54. Ebenso E.E., Obot I.B., Murulana L.C., *Int. J. Electrochem. Sci.*, 5 (2010) 1574.
55. Migahed M.A., *Mater. Chem. Phys.*, 93 (2005) 48.
56. Wang X., Yang H., Wang F., *Corros. Sci.*, 53 (2011) 113
57. Cano E., Polo J.L., La IglesiaA., Bastidas J.M., *Adsorption*, 10 (2004) 219-225.
58. BentissF., Lebrini M., Lagrenée M., *Corros. Sci.*,47 (2005) 2915.
59. Li X., Deng S., Fu H., *Corros. Sci.*, 53 (2011) 302.
60. Ozcan M., Solmaz R., Kardas G., Dehri I., *Colloid Surf. A*, 57 (2008) 325.
61. Bockris J.O'M., Reddy A.K.N., *Modern Electrochemistry*, vol. 2, Plenum Press, New York, 1977.
62. Wang L., *Corros. Sci.* 48 (2006) 608–616.
63. Benabdellah M., Aouniti A., Dafali A., Hammouti B., Benkaddour M., Yahyi A., Ettouhami A., *Appl. Surf. Sci.* 252 (2006) 8341–8347.
64. Benabdellah M., Benkaddour M., Hammouti B., Bendahhou M., AounitiA., *Appl. Surf. Sci.* 252 (2006) 6212–6217.
65. Martinez S., Stern I., *Appl. Surf. Sci.* 199 (2002) 83–89.
66. Szauer T., Brandt A., *Electrochim. Acta* 26 (1981) 1253–1256.
67. Guan N.M., Xueming L., Fei L., *Mater. Chem. Phys.* 86 (2004) 59–68.
68. El Ouali I., Hammouti B., Aouniti A., Ramli Y., Azougagh M., Essassi E.M., Bouachrine M., *J. Mater Environ. Sci.* 1 (2010) 1–8.
69. Morad M.S., Kamal El-Dean A.M., *Corros. Sci.* 48 (2006) 3398- 3412.
70. Kalil N., *Electrochim. Acta.* 48 (2003) 2635–2640.
71. Rameshkumar S., Danae I., Rashvand Avei M., Vijayan M., *J. Mol. Liq.* 212 (2015) 168-186.
72. Sastri V., Perumareddi J., *Corrosion.* 53 (1997) 617-622.
73. Pearson R.G., *Inorg. Chem.* 27 (1988) 734-740.
74. Martinez S., *Mater. Phys.* 77 (2003) 97-102.
75. Lukovits I., Kalman E., Zucchi F., *Corrosion.* 57 (2001) 3-8.
76. Rodriguez-Valdez L.M., Villamisar W., Casales M., Gonzalez-Rodriguez J. Martinez-Villafañe A., Martinez L., Glossman-Mitnik D., *Corros. Sci.* 48 (2006) 4053-4064.
77. Li X., Deng S., Fu H., Li T., *Electochimica Acta.* 54 (2009) 4089-4098.
78. Feng L., Yang H., Wang F., *Electochimica Acta.* 58 (2011) 427-436.
79. Jafari H., Sayin K., *J. Taiwan Inst. Chem. Eng.* 56 (2015) 181-190.
80. Saha S.K., Ghosh P., Hens A., Murmu N.C., Banerjee P., *Phys. E Low-Dimens. Syst. Nanostructures.* 66 (2015) 332-341.
81. Mi H., Xiao G., Chen X., *Comput. Theor. Chem.* 1072 (2015) 7-14.
82. Kaya S., Tüzün B., Kaya C., Obot I.B., *J. Taiwan Inst. Chem. Eng.* 58 (2016) 528-535.
83. Eivani A.R., Zhou J., Duszczuk J., *Comput. Mater. Sci.* 54 (2012) 370-377.
84. Kaya S., Kaya C., Guo L., Kandermirli F., Tüzün B., Uğurlu İ., Madkour L.H., Saraçoğlu M., *J. Mol. Liq.* 219 (2016) 497- 504.
85. Khaled K., El-Maghraby A., *Arab. J. Chem.* 7 (2014) 319-326.